Proposal to Study 6D Cooling with an Achromatic Ring, Injection and Extraction, Final Cooling with a 40T Solenoid and Various Heating Simulation (Wedge, Collider Magnets) by the UCLA MAP Team

Principal Investigator: **Professor David B. Cline**
Department of Physics and Astronomy
University of California, Los Angeles
475 Portola Plaza
Los Angeles, CA 90095-1547
Telephone No. 310-825-1673
e-mail: dcline@physics.ucla.edu

1. Introduction

Our current main research includes aspects of simulation studies on 6D cooling of muon beams. There are several on novel concepts in our muon 6D cooling effort such as the first study of an achromatic solenoid dipole ring cooler. With the help of Al Garren we study the lattice of the muon collider using open mid-plane dipoles. All our muon collider projects have been included in the MAP program to date.

During the past two years the muon collider and neutrino factory group has been reorganized into the FNAL-led Muon Acceleration Program (MAP). Recently this project was included in the FY 12 president's budget and a letter of approval has been sent by the DOE. The UCLA team has been recommended for MAP supplemental funding by the MAP leadership and had signed a SOW for our activity that will be discussed during this proposal. We hope this will continue during the duration of the current proposal.

In the past year, we have concentrated on the MAP program and made significant progress. We published one paper of "6D $\mu\pm$ cooling using a solenoid-dipole ring cooler for a muon collider" in Oct. 2011 issue of NIMA journal. Another paper of "Optimization of a mercury jet target for a neutrino factory or a muon collider" will also be published in Nov. 2011 issue of PRSTAB journal. There are also several key proceedings, notes and talks from our group and they are listed in the following.

1. Al Garren, J.S. Berg, D. Cline, X. Ding, H.G. Kirk, "Robust 6D $\mu\pm$ cooling using a solenoid-dipole ring cooler for a muon collider", Nuclear Inst. and Methods in Physics Research, A 654   (2011) 40-44.

2. X. Ding, D. Cline, H.G. Kirk and J.S. Berg, "Optimization of a Mercury Jet Target for a Neutrino Factory or Muon Collider", BNL-96471-2011-JA, MAP-doc-4313, IDS-NF-AWG-004, 2011 (in Press at Physics Review Special Topics - Accelerator and Beams).

3. D. Cline, X. Ding, A.A. Garen, F.Mills, "Estimate of the parameters for the injection system into the solenoid/dipole ring cooler and the heating of the cooling absorbs", MAP-doc-4304, 2011.

4. X. Ding, D. Cline, A.A. Garren, H.G. Kirk, J.S. Berg, "Status of studies of Achromat-based 6D Ionization Cooling Rings for Muons", IPAC11, MOPZ030, San Sebastian, Spain, 2011.

5. R. Palmer, R. Fernow, Jon Lederman, "Muon collider final cooling in 30-50 T solenoids", in Proceedings of PAC 11, New York, 2011. (BNL-94919-2011-CP)

6. X. Ding, D. Cline, A. Garren, H. Kirk, J.S. Berg, "Robust 6D muon cooling in four-sided ring cooler using solenoids and dipoles for a muon collider" in Proceedings of PAC 11 (MOP055), New York, 2011.

7. X. Ding, D. Cline, A. Garren, H. Kirk, J.S. Berg, "Racetrack muon ring cooler using solenoids and dipoles for a muon collider", in Proceedings of PAC 11 (MOP054), New York 2011.

8. R. Weggel, D. Cline et al., "Open Midplane Dipoles for a Muon Collider" in Proceedings of PAC 11 (TUP177), New York, 2011.

9. D. Cline, "A/H Higgs Factory, Possible CP Violation and 6D Cooling", Muon

Collider 2011 (Physics-Detectors-Accelerators), Telluride, June 27-July 1, 2011.

10. H. Kirk, X. Ding, "Power Deposition in the Open Middleplane Dipole", Muon Collider 2011 (Physics-Detectors-Accelerators), Telluride, June 27-July 1, 2011.

11. X. Ding, "Power Density Study for Open Midplane Dipole", MAP Collider Ring Magnets Mini-Workshop, FNAL, May 19-20.

12. D. Cline, "Search for A/H at LHC and Implication for a Muon Collider Higgs Factory", Muon Accelerator Program-Winter Meeting, Jefferson Lab, Feb. 28-March 4, 2011.

13. X. Ding et al., "Advances for a Solenoid/Dipole 6D Cooling Ring", Muon Accelerator Program-Winter Meeting, Jefferson Lab, Feb. 28-March 4, 2011.

14. Jon Lederman, "Final Cooling Studies", Muon Accelerator Program-Winter Meeting, Jefferson Lab, Feb. 28-March 4, 2011.

15. A. Garren, "6D Cooling Ring Lattice Strategies", Muon Accelerator Program-Winter Meeting, Jefferson Lab, Feb. 28-March 4, 2011.

16. K. Lee et al., "Simulation Study of Solenoid-Lithium Lens Channel", Muon Accelerator Program-Winter Meeting, Jefferson Lab, Feb. 28-March 4, 2011.

17. K. Lee, D. Cline, A. Garren, "Study of Li Lens Channel for Final Muon Ionization Cooling Stage", MAP note, 2011

1.1 Past work

Over the past decade we have been working on variants of 6D final muon cooling or muon collider R&D: A solenoid/dipole ring cooler; a Li lens final cooler; a final cooler that uses high field solenoids (40-50T); the open midplane dipole and the lattice of the collider; studies of the target optimization for the $\mu\pm$ production; and the MICE project.

We are working on developing components for the following so-called Neuffer-Fernow plot that shows the required transverse and longitudinal emittance for a muon collider. Our major goal is to reach the emittance needed for a muon collider Higgs factory or higher energy muon collider. Work has been done largely in collaboration with the group at BNL and the company Particle Beam Lasers Inc. and the MAP team. The modern muon collider was started in 1992 based on ideas of Budker and Skrinsky at a much earlier time. For the first ten years we had extensive numbers of workshops, many organized by UCLA and concentrated on transverse muon cooling, believing that this was the easier cooling process.

New schemes are needed for final transverse cooling. One is to use a Li lens final cooler, which we describe below. The other is a string of very high field solenoids (~40-50T) to achieve the final cooling. Our group is working on both methods and this will be described later in the proposal and is the PhD thesis work of Jon Lederman.
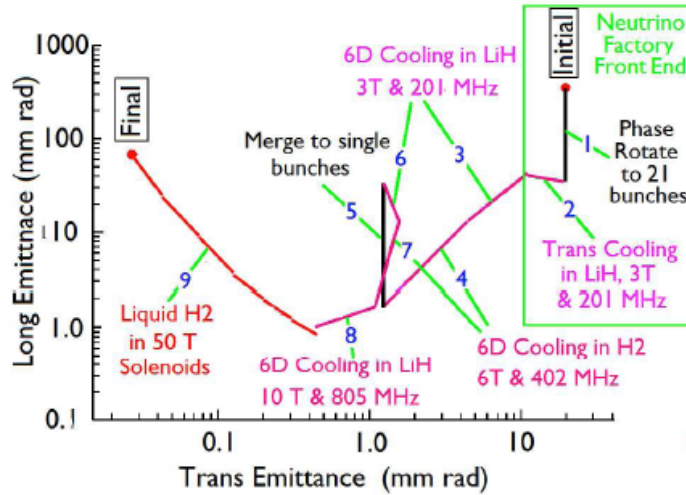
Figure 1. A complete scheme of ionization cooling for a muon collider.

1.2 Physics motivation for a muon collider

The motivations for building a muon collider are considerable. Such a machine promises the exploration of new physics by expanding the energy frontier. A muon machine also provides a fertile environment for studying Higgs physics, SUSY and CP violation. The coupling to the S channel is larger by M_μ^2/M_e^2.

Higher Energy Physics Studies: Reduced synchrotron radiation allows for more focused acceleration of muons than electrons. Because muons are point particles, they offer advantages over composite particles such as hadrons.

Higgs Factory: This idea was formed in our first UCLA workshop in 1992. The theorized Higgs particles, which may be discovered at the LHC, are responsible for the generation of mass for fermions via the Yukawa couplings. Muons are strongly coupled to the hypothesized Higgs particles.

SUSY: A special type of Higgs Bosons are predicted, A and H. We have been a strong proponent of the A/H muon collider Higgs factory.

1.3. 6D muon cooling

In order to maximize the event rate, the goal is to maximize the luminosity at the interaction point. In order to achieve maximum luminosity, the emittance of the beam in both transverse and horizontal dimensions should be as low as possible. Accordingly, the final stage of the muon collider is 6D cooling, which is designed to reduce the beam emittance. 6D cooling refers to the reduction of the phase space volume of the muons. Muon cooling presents significant technical challenges due to the fact that the muon lifetime is on order of microseconds and thus the cooling must occur on this timescale.

The theory of ionization cooling demonstrates that reduction of transverse emittance also brings about heating in the longitudinal dimension. The longitudinal heating is directly related to the negative slope of the $\dfrac{dE}{dz}$ (relative ionization) curve. Thus, in the final cooling, maximizing the luminosity requires reducing the transverse

emittance while minimizing the growth of the longitudinal emittance. Because the transverse emittance is proportional to the beta function, it is desired to reduce the beta function of the beam.
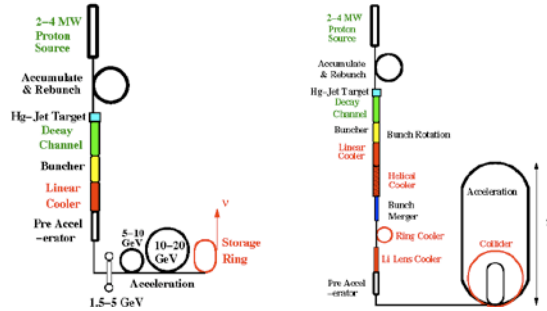

Figure 2. Schematic drawings from the Muon Collider MAP in a) schematic of 20 GeV NF and in b) schematic of 1.5 TeV MC.

Table 1. Parameters for two muon collider options.

c.m. Energy	1.5 TeV	4 TeV
Luminosity ($cm^{-2}sec^{-1}$)	1×10^{34}	2×10^{34}
μ's per bunch	2×10^{12}	2×10^{12}
Ring Circumference (km)	3.0	8.1
Betatron at IP (mm)	10	3
r.m.s. $\Delta p/p$	0.001	0.0012
Repetition Rate (Hz)	12	6
$\varepsilon_\perp$ ($\pi \cdot mm \cdot mrad$)	25	25
$\varepsilon_\parallel$ ($\pi \cdot mm \cdot mrad$)	72,000	72,000

Since 2010 the previous collaboration has been subsumed into the MAP program that is now approved by the DOE. All of the methods studied in this proposal were in the MAP proposal and are consistent with the current MAP program.

2. MICE: Recent progress on the international muon ionization cooling experiment

The UCLA members have been involved in the Muon Ionization Cooling Experiment (MICE) from the initial conception in 2000. X. Yang helped Alan Bross with the tracker development. D. Cline and K. Lee will help with the MICE data analysis. X. Yang will take shifts.

The muon beam at the Rutherford lab will be low enough intensity for the trackers. Over the two decades of simulation studies show that there will be transverse cooling. The R&D experiment will not only verify the known results from simulation studies but also will be a significant development project of the necessary technology

towards a future Neutrino Factory or a muon collider construction. Our funding has been tight so we have had problems paying the MICE fee. We hope to send some funds now.
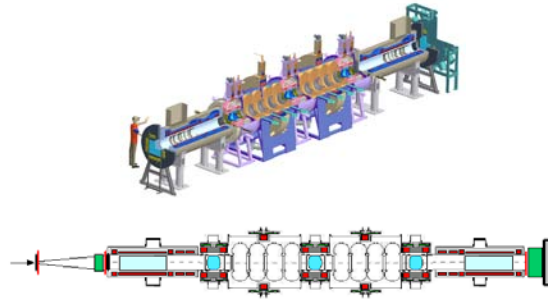

Figure 3. MICE channel 3-D and schematic layouts.

3. Research progress on 6D muon cooling with a Dipole-Solenoid ring

6D ionization cooling of muons is needed to achieve the necessary luminosity for a muon collider. If that cooling could occur over multiple turns in a closed ring, there would be significant cost savings over a single-pass cooling channel. We propose to use a ring that employs both dipoles and solenoids with the additional requirement that the arcs of the ring to be achromatic. We find robust 6D cooling in the simulation.

The lattice design has evolved from the original concept shown in Fig. 4 (left) to a lattice design that is much more effective for cooling by Al Garren. Our first design of an achromatic cooling lattice, which had a two-sided "racetrack" shape, had rather poor cooling performance. We identified two causes for this: a very low dynamic aperture, and a small momentum passband. Particles that were being lost showed significant signs of coupling between the transverse and longitudinal planes. Furthermore, since the minimum of the time of flight as a function of momentum was at a relatively low momentum, we were forced to operate at a low momentum (145 MeV/c) to stay on one side of the minimum so as to have synchrotron oscillations. These observations, plus experience from the RFOFO cooling ring that dynamic aperture was reduced when there was more bending, led us to reduce the dispersion in the ring by using a four-sided shape, but otherwise the same structure. This would allow us to operate at a higher momentum, improving the sum of the damping partition numbers. We also designed the lattice so the design tune was 1.75 (instead of the original 1.68), so as to center the design momentum in the passband. The dynamic aperture did not improve when we did this, indicating that the dynamic aperture was dominated by the solenoid part of the lattice, and that the symmetry breaking from the bending was a minor contribution.

We then made a modified lattice where each superperiod was close to having an internal eight-fold symmetry. The original lattice lacked this symmetry since it was desirable to have a long distance between solenoids in the straight sections to allow space for injection and extraction hardware, while it was desirable to have low beta functions at the absorbers in the arcs. The resulting lattice had a significantly improved dynamic aperture, and a significantly improved momentum passband arising from the reduced chromaticity of the lattice. In addition, we used a four-sided lattice to improve the sum of the damping partition numbers as described above. The resulting cooling performance was a significant improvement over that of the original lattice.
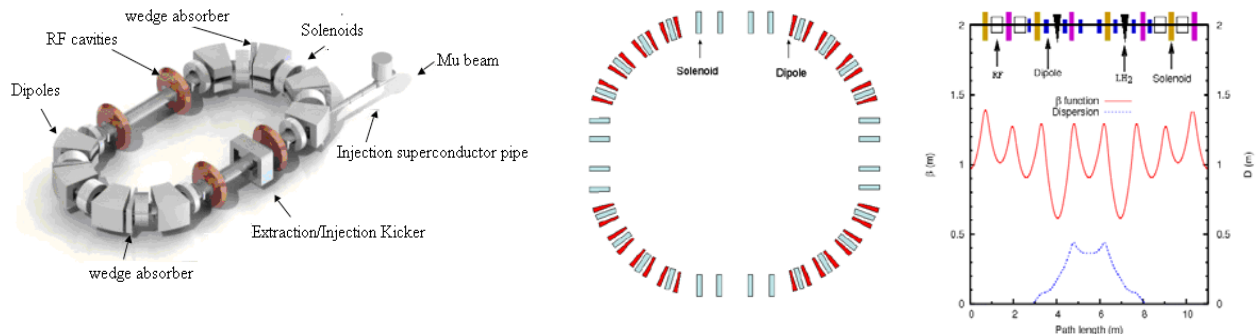
6

Figure 4. Schematic drawing of the racetrack (left) and four-sided Solenoid-Dipole ring (middle) and beta function and dispersion in a ring quadrant of four-sided ring (right).

The four-sided ring is shown in Fig. 4. It has four 90 deg arcs and 8 dipoles separated by solenoids in each arc. The arcs are nearly achromatic both horizontally and vertically. The result is that the dispersion is zero in the straight sections between the arcs. In order to cool the beam, the liquid hydrogen (LH$_2$) wedge coolers are inserted into a region with low β and high dispersion. For each LH$_2$ wedge absorber, it has a length of 19.5 cm, energy loss rate of 0.3 MeV/cm and wedge angle of 23 deg. Four 201.25 MHz accelerating cavities (RF) are placed in the superperiod. Its accelerating gradient is 15 MV/m and RF phase is 30 deg. The RF cavities will restore the energy of muon beam lost in the LH$_2$ absorbers. Our compact four-sided ring has positive dispersion, which means that higher momentum particles have longer paths around the ring, and thus lose more energy per turn, than the low energy particles do. Consequently, cooling takes place in the longitudinal as well as the transverse dimensions. Evolution of the beam parameters in the cooling process during 15 turns of the four-sided ring cooler is presented in Fig. 5. If we time the entire horizontal, vertical and longitudinal invariant emittance together, we see the 6D emittance has fallen by a factor 31.9 after 15 revolutions with a transmission of 42% (64% without muon decay) and the Merit factor is 13.2. So we see there is a robust 6D cooling for the circulating muon beam in each of the three space and three momentum dimensions [1].
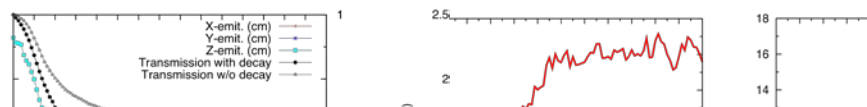

Figure 5. Beam emittance and transmission (left) and Merit factor (right) as a function of full ring turns. Note that the figure of merit has greatly improved.

References

1. Al Garren, J.S. Berg, D. Cline, X. Ding, H.G. Kirk, "6D $\mu^{\pm}$ cooling using a solenoid-dipole ring cooler for a muon collider", Nuclear Inst. and Methods in Physics Research, A 654 (2011) 40-44.

4. Study on injection scheme of the Dipole-Solenoid ring cooler

Now we look at the injection requirement of the above dipole-solenoid ring cooler [1, 2]. First, as shown in Fig. 6, we increase the length of solenoids in the straight section of original lattice in Fig. 1 from 0.25 m to 0.5 m. This will keep the circumference and the 6D cooling behavior no change. But it can reduce the hard edge focusing of solenoids and make the larger deflected beam by the kicker go through this solenoid without being lost. Second, we simulate the real beam from our previous 6D cooling study with normalized horizontal emittance of 1.26 cm and vertical emittance of 1.48 cm and its plot of X-Y and Px-Py at the beginning of first straight section before the K1 is shown in Fig. 7. Our simulation (see Fig. 8) shows we can't obtain necessary separation in front of the Sol2 if this entire initial beam is launched. In our lattice, a 90 degrees in betatron phase is already designed for some point in the straight section in front of the Sol2 relative to the middle point of the kicker.

We found the high horizontal momentum is harmful for the separation between the extracted beam and circulating orbit. By limiting the Px to 0.03 GeV/c to pick out the remaining 85% from the entire initial beam, we found a clear separation between this beam and the circulating orbit. Fig. 9 show this simulating result and we see this selected beam can be tracked and arrive at the location in 100% just before the second solenoid with a clear separation for inserting the flux tube. By the way, we found the strength of 1st kicker (K1) can be neither too high nor too low. If too low, the deflection is not enough for separation in the following straight section. If too high, the solenoids will bring some beam to center axis in negative slope in the following straight section. Our best value of K1 and K2 in the beam case is around 0.28 T and 0.65T, respectively.

Because a solenoid will rotate the median plane and give the beam a tilt, the r-z plot in Fig. 9 can't exactly reflect the real beam separation between the injected/extracted beam and closed orbit. We must use x-y plot to directly see if the beam is separated or not in space. Fig. 10 is a x-y plot at the end of K2. We see the beam has already enough separation using only strength of 0.3 T for each of K1 and K2.

In conclusion, we have simulated the extraction process with both single particle and the beam. We find two kickers and a superconducting flux exclusion tube are required in our extraction system. At this stage, our simulation shows a clear separation can be created in front of the Sol2 between the extracted beam from 85% of the entire initial beam for 6D cooling and the circulating orbit. The injection is exactly a reverse of extraction process. So we can envision the beam can be injected from the right to left inside this flux exclusion tube, go through the Sol2 with field-free path and then merged into the cooling orbit utilizing two kickers.

References

1. Al Garren, J.S. Berg, D. Cline, X. Ding, H.G. Kirk, "6D $\mu^{\pm}$ cooling using a solenoid-dipole ring cooler for a muon collider", Nuclear Inst. and Methods in Physics Research, A 654 (2011) 40-44.

2. D. Cline, X. Ding, A.A. Garen, F.Mills, "Estimate of the parameters for the injection system into the solenoid/dipole ring cooler and the heating of the cooling absorbs", MAP-doc-4304, 2011.
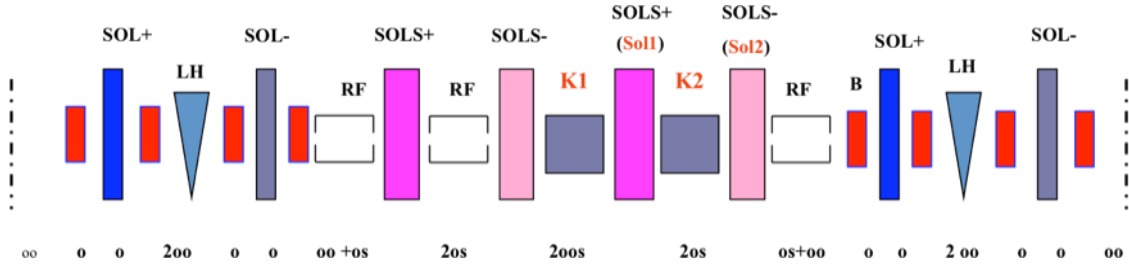
Fig. 6. Layout of K1, K2, Sol1 and Sol2 for injection/extraction (Modified lattice with 0.5m of solenoids in straight section).
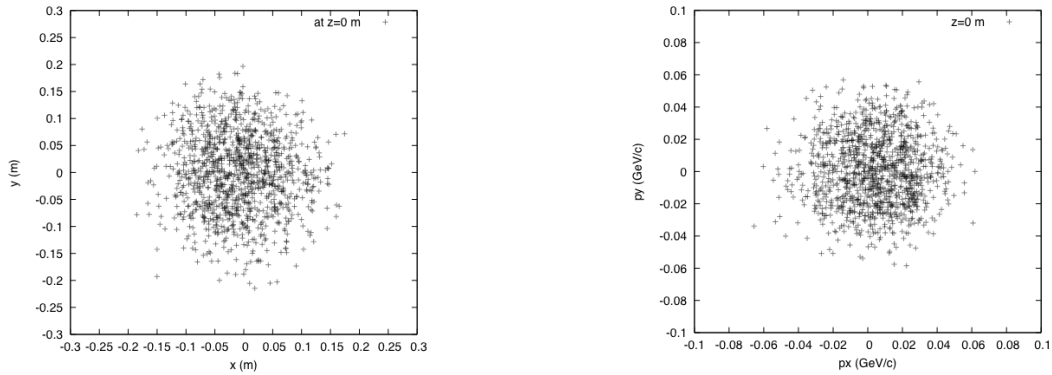
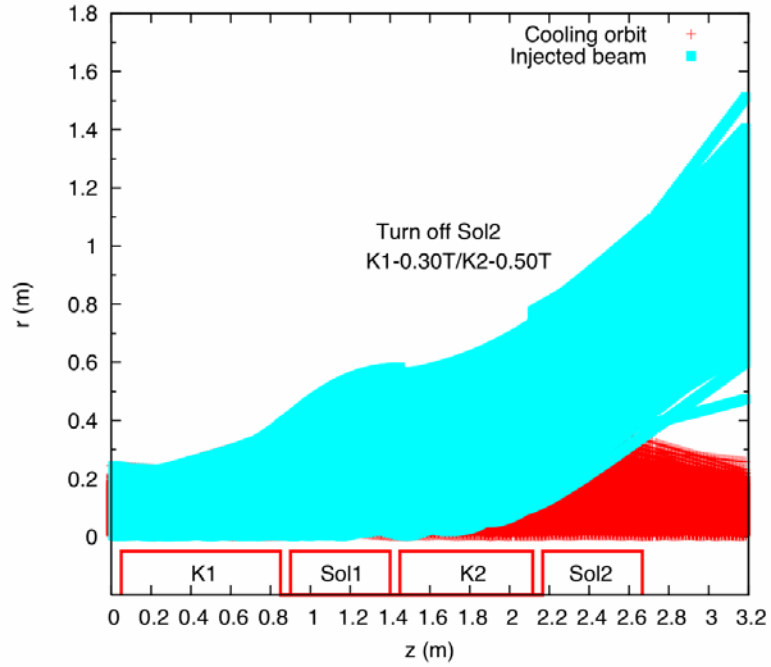**Fig.7. Plot of X-Y and Px-Py with initial beam found in the 6D cooling study.**

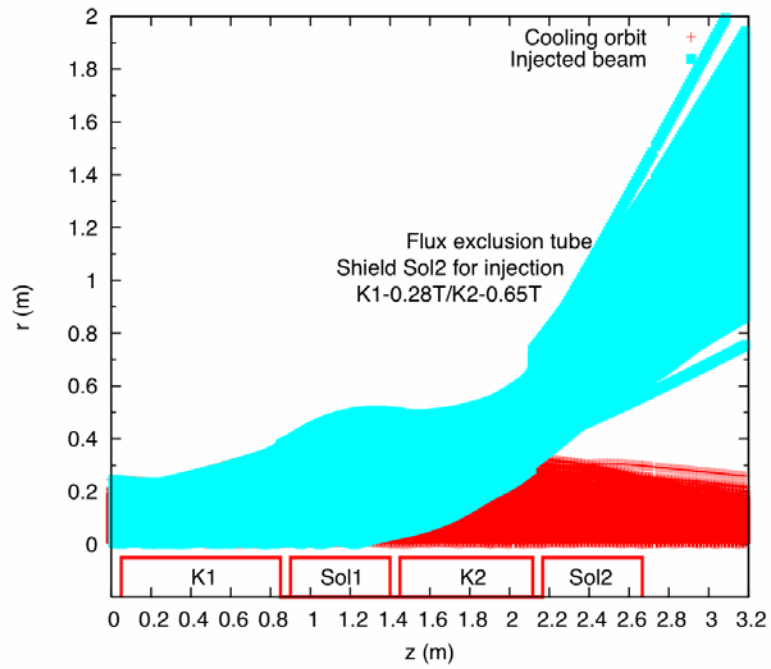**Fig. 8. Simulation of the initial entire beam for injection/extraction.**

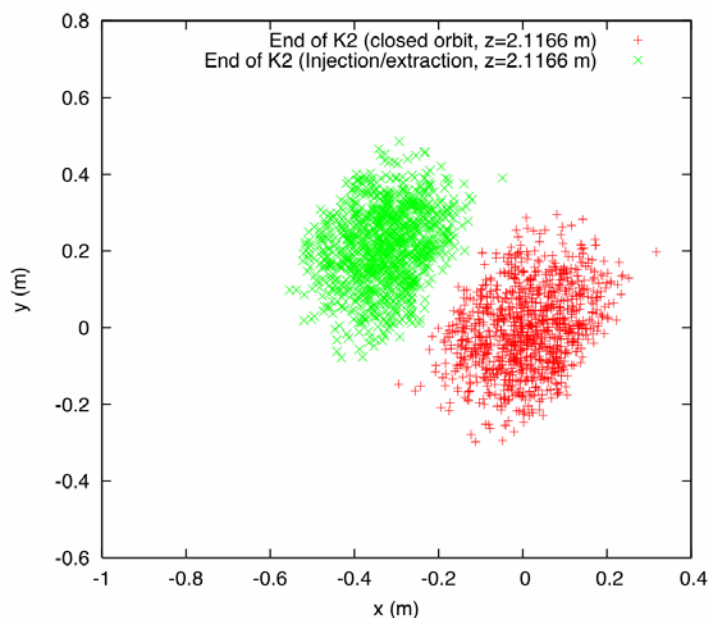**Fig. 9. Simulation of 85% of the initial entire beam for injection/extraction (r-z plot).**

Fig. 10. Simulation of 85% of the initial entire beam for injection/extraction (x-y plot).

5. Final cooling with PBL-BNL 40T magnet and simulation of full channel with RF

6D coolers do an excellent job of cooling in the longitudinal emmittance but fail to give strong transverse cooling. For a muon collider small transverse emmittance is crucial. For this reason the MAP group is studying additional transverse cooling or final cooling. In order to give strong final cooling a system of very low β is needed. The leading system is to use very high field solenoids (50T) to produce this low β. Coincidentally the PBL Company is developing a 40T system under an SBIR grant.

Jon Lederman will do his PhD thesis on the study of this cooling. Due to space restriction in this proposal we cannot lay out the full calculations involved. One is an attempt to lower the magnetic field.

One use of this final cooling is to produce a Higgs factory muon collider. D. Cline has proposed that the A/H Higgs Boson could be studied with such a collider and possibly discovers the origin of CP violation in nature.

We propose a final cooling scheme utilizing lower momenta, which allows for operating at lower magnetic fields. The transverse emittance may then be reduced using progressively higher solenoid fields to drive down the beta function. Operating at lower energy also reduces the beta function.

Operating at lower momentum, however, introduces longitudinal heating because this translates to operating at progressively higher negative slopes on the dE/dz curve. Longitudinal emittance growth is also caused by energy straggling and bunch length growth due to time of flight effects.

Fig. 1 shows a plot of longitudinal emittance vs. transverse emittance for a muon collider. The final cooling (shown by the red line toward the left of the plot) depicts the final cooling. Note that the reduction of transverse emittance is accompanied by grown
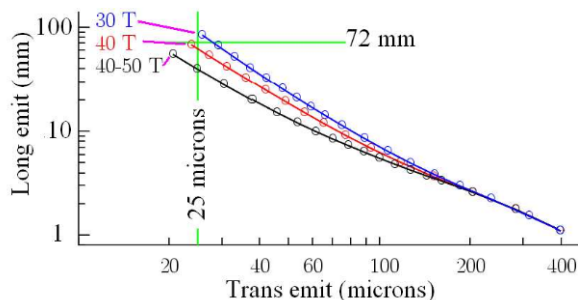
in longitudinal emittance due to the longitudinal heating effects described above (see Figure 1 for reference).

Fig. 11 shows one final cooling stage. The stage includes a liquid hydrogen absorber to achieve ionization cooling followed by a drift section and then an RF linac to restore the energy lost in the transverse dimension. The focusing is achieved via solenoid fields. The field flip is introduced in order to reduce the accumulation of canonical angular momentum.

Fig. 12 is a plot of longitudinal emittance vs. transverse emittance for a final cooling channel (the plot should be read left to right in moving along the cooling channel). Thus, this data reflects a series of cooling stages. The data was generated without simulating full RF for each stage. Instead, the RF effects were generated manually.

Note that the higher fields curves exhibit lower slope and thus lower longitudinal emittance growth. Based upon the plot in Fig. 12, it is clear that the desired emittance goals may be achieved with 50T solenoids. However, importantly, the simulations results also show the emittance goals may be reached with 40T solenoids and possibly 30T solenoids. This is a significant simulation result for it indicates the more technically challenging 50T solenoids may not be required for final cooling.

References

1. Cline, David, Search For A/H at LHC and Implication for a Muon Collider Higgs Factory, JLAB Winter MAP Meeting, March 3, 2011.

2. Palmer, Robert, A Complete Scheme Of Ionization Cooling For A Muon Collider, arXiv:0711.4275v1 [physics.ac-ph], November 27, 2007.

Figures 11. Final cooling scheme using 50T solenoids.

Figure 12. The different transverse emittances for a high field final cooler.

6. Study of the constraints on a muon collider for a study of the A/H Higgs Bosons

The current status of the search of the standard model Higgs boson is this: both CMS and Atlas have limited the Higgs to be less than 140 GeV to 95 percent confidence level. There is excess of background and signal in the 120 GeV region where the standard model Higgs should exist. It will take some time to sort this out.

Other teams are searching for the A Higgs boson (UCLA et al). This may be easier than the low mass Higgs. Should the A be discovered we have shown long ago that the A and H having different CP status could interfere in indicating large CP violation. This could in part motivate an S channel Higgs boson.

After the study we will submit a paper to Phys. Rev. Letters. Jon Lederman will include this in his PhD thesis at UCLA (with Gail Hanson).

7. Simulation of meson production on the muon collider target

We have been asked by the MAP team to work with the target studies to perform the pion production simulation for a 4-MW target station. Using the MARS code, we simulate particle production initiated by incoming protons below with kinetic energies between 2 and 100 GeV. For each proton beam energy, we optimize particle production by varying the target parameters: the mercury jet radius, the incoming proton beam angle, and the crossing angle between the mercury jet and the proton beam. With an 8 GeV proton beam, we study the variation of meson production with the direction of the proton beam relative to the target. In addition, the correlation between pion production and multiple beam entry points for the proton beam onto the jet has been examined. We also examine the influence on the meson production by the focusing of the proton beam. Finally, the number of muons surviving through the Neutrino Factory front end channel is determined as a function of the proton beam energy.

Recently, we have revised our optimization procedure to make sure the proton beam always exactly below the mercury jet when the beam approaches the jet at the intersection point of z=-37.5 cm. We are also required to study the meson production with the Ga target. In the second year of MAP, we will optimize the target parameters for both cases of HG and GA target with kinetic energies between 2 and 15 GeV in order to compare their performance. In addition, H.G. Kirk et al. developed a new target system baseline [2] for a Muon Collider or a Neutrino Factory. This revised baseline requires a

new configuration of the target SC magnets. We will also perform the meson production simulations and optimization studies of target parameters for this new configuration.

References

1. X. Ding, D. Cline, H.G. Kirk and J.S. Berg, "Meson Production Simulations for a Mercury Jet Target for a Neutrino Factory or Muon Collider", (in Press at Physics Review Special Topics - Accelerator and Beams).
2. H.G. Kirk et al., http://physics.princeton.edu/mumu/target/target_baseline_v3.pdf

8. Heating study of muon collider ring dipole with shielding pipe or open midplane

A key R&D component in MAP is the design of muon collider lattice and the development of the technology required to cope with radiation from the decay of muons circulating in the collider ring. In 1995 the first study of the lattice of a muon collider was carried out by A. Garren et al. Very recently, the MAP is very interested in the study of superconducting magnets for the collider and Alexahen et al. have studied the new candidate lattices. To shield the magnets from the radiation of energetic synchrotron photons and electromagnetic showers, we've studied the open-midplane dipole (OMD) with no conductor near the plane of the accelerator or storage ring, where most of the muon decay takes place. Our preliminary simulation (see Fig. 13) using MARS15 for a unidirectional muon beam exiting an open-midplane dipole of 6-m length and 15-mm half-gap shows the peak power density on SC coils is within the nominal quench limit of 1.6 mW/g [1, 2].

In addition to OMD, there are two different shield and dipole magnet concepts are proposed. The first would have an elliptical tungsten shield pipe within an elliptical 'cosine theta' dipole magnet. The second concept would be for a rectangular room temperature tungsten shield pipe within a new 'Inside Support Free' rectangular block dipole, using concepts from Open Mid-Plane designs.

We will continue our study of muon collider ring dipole with shielding pipe or OMD. We will set up a simulation, using the MARS code, of the energy leakage from the different design. Our goal is to iterate the designs until the specification of less than 1 % leakage is achieved with the minimum shield dimensions. Al. Garren and R. Weggel will be the lead person in advising and establishing the ring lattice and ring dipole parameters to provide better specification of dynamic aperture and field-quality requirements.

We will help R. Palmer with study of the Tungsten fill collider magnet.
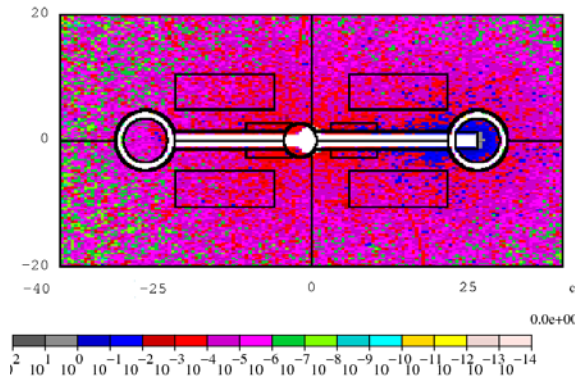

Figure 13. Energy deposition at the downstream end of a 6-m-long OMD.

References

1. R. Weggel, D. Cline et al., "Open Midplane Dipoles for a Muon Collider" in Proceedings of PAC 11 (TUP177).
2. N.V. Mokhov, et al., "Energy Deposition Limits in a Nb3Sn Separation Dipole in Front of the LHC High-Luminosity Inner Triple," PAC, Portland, USA, May 2003.

9. Proposed progress over a year

The approval of the MAP program by the DOE has been a dream of ours since our first meeting in 1992. MAP funds at UCLA are focused on the muon collider design studies. Activities include simulations of muon collider cooling channels, including cooling rings and the 40T final cooling channel. Other work includes optimization studies for high-power MC/NF targets and energy deposition in collider ring targets.

The supervision of the team at BNL is made by H. Kirk (Ding, PhD student Lederman).

The SOW between FNAL and UCLA for the next year could include (see Table 2):

Table 2. Muon collider and cooling research

6D ring cooler using dipoles/solenoids	Goal: To reach a merit factor of 100 (D. Cline, <u>X. Ding</u>, A. Garren, K. Lee, BNL group) to advance the state of the injection/extraction system design.
The heating of muon collider ring dipole and muon collider lattice	Goal: To study the heating due to the circulating muon beam for several ring dipoles in a row (D. Cline, <u>X.Ding</u>) to study a modified lattice to reduce the heating (Al. Garren and BNL group)
The injection and extraction into the ring cooler	Goal: To continue the injection studies started last year and described in Fig. 8/9 (<u>K.Lee</u>, X. Ding, D. Cline, BNL Collaboration)
The study of final cooling using high field solenoids	Goal: To simulate the transverse emittance using high field solenoids (<u>J. Lederman</u>, PhD student, D. Cline, R. Palmer, J.S. Berg)
The MICE project	Goal: To take shifts and help analyze data (<u>X. Yang</u>, K.Lee, D. Cline)
Target studies	Goal: To assist the BNL group in studies of muon production with a mercury jet and GA target (<u>X.Ding</u>, BNL group)
Study of the Constraints on a Muon Collider for the Study of the A/H Higgs Bosons	Goal: To study the parameters of an S channel muon collider for CP violation at the A/H particles (<u>D. Cline</u>, J. Lederman, Gail Hanson)

10. Budget

11. Appendix (key papers in the past year)

6D $\mu^{\pm}$ cooling using a solenoid-dipole ring cooler for a muon collider

Al Garren [b], J.S. Berg [a], D. Cline [c], X. Ding [c,*], H.G. Kirk [a]

[a] *Brookhaven National Laboratory, Upton, NY 11973, USA*
[b] *Particle Beam Lasers, Inc., Northridge, CA 91324, USA*
[c] *UCLA, Los Angeles, CA 90095, USA*

ABSTRACT

Six dimensional cooling of large emittance μ^+ and μ^- beams is required in order to obtain the desired luminosity for a muon collider. We propose to use a ring cooler that employs both dipoles and solenoids with the additional requirement that the arcs of the ring be achromatic. We describe the lattice and the beam dynamics of the proposed ring, and demonstrate that the lattice gives substantial cooling in all 6 phase space dimensions.

© 2011 Elsevier B.V. All rights reserved.

1. Introduction

A $\mu^+\mu^-$ collider could provide new opportunities, both as a discovery machine as well as providing for precision testing of potential LHC discoveries such as SUSY Higgs particles (200–600 GeV) in the s channel and new high mass particles such as Squarks (TeV) [1]. Further, a $\mu^+\mu^-$ collider could be placed on established laboratory sites such as FNAL, BNL, or CERN (Fig. 1).

The Muon collider concept was first deemed to be practical when it was realized that a collected muon beam could be cooled by a process utilizing energy losses during the beams passage through an appropriate material [2–4]. In this technique, referred to as ionization cooling, the magnitudes of 3-dimensional momentum vectors of each of the muons are reduced via energy loss in an ionizing medium followed by the subsequent restoration of only the longitudinal momentum component utilizing RF cavities. The attainment of this cooling reduces the beam emittance, which leads ultimately to a useful luminosity in the muon collider.

The modern vision of a high-luminosity machine was developed by Neuffer and Palmer in 1994 [5]. Subsequently, it was realized that a muon storage ring could produce a powerful neutrino beam [6] and this idea was further developed into the concept of a neutrino factory [7]. Key differences between the muon collider and neutrino factory are that a muon collider requires substantially more cooling and that the cooling for a muon collider should apply to the full six dimensional phase space of the beam. In order to realize longitudinal cooling via the energy loss process, it is necessary for the beam to have

dispersion. This is because dispersion gives the beam a correlation between energy and transverse displacement. The placement of absorbing wedges in the beam creates a favorable correlation between particle energy and energy loss, and this allows longitudinal cooling.

Most scenarios currently envisioned for a muon collider envision a single-pass cooling system. Such a system requires a large number of RF cavities and their power supplies to restore the energy lost in the absorbers during the ionization cooling process, as well as the associated focusing magnets for the system. This will make the cooling system a substantial fraction (if not the majority) of the cost of a muon collider. If one could re-use that hardware, by making multiple passes through the RF cavities and absorbers, one would expect to substantially reduce the cost of a muon collider. The ideal way to achieve such re-use would be to cool in a ring, where one injects the beam into the ring, allows the beam to cool for some number of turns, then extracts the cooled beam.

Several authors have studied such cooling rings. The first ionization cooling ring for muons that was studied significantly was a racetrack-shaped ring, which ran on a linear resonance [8]. The performance of a solenoid-focused ring working on that principle was limited by chromaticity, which meant that off-energy particles would not be on that linear resonance [9]. A later solenoid-focused design by Balbekov [10,11] did not rely on running on the linear resonance, and achieved good performance with an idealized field model. Unfortunately, once more realistic fields were included, particularly in the field flip region, the performance suffered significantly [12,13]. Furthermore, removal of RF cavities to allow for injection and extraction resulted in significantly degraded performance [11].

* Corresponding author. Tel.: +16313442042.
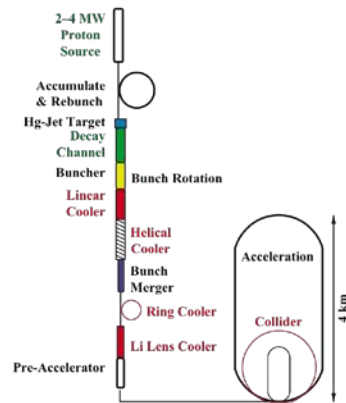*E-mail addresses:* xding@bnl.gov, dingxp@live.com (X. Ding).

Fig. 1. Schematic diagram of a $\mu^+\mu^-$ collider.

Other authors have studied rings that used either quadrupoles or weak/edge focusing in dipoles [14–17]. These rings had a wide range of performance, but suffered from lacking any provision for injection and extraction. For the designs that used dipole edges for focusing, the designed fields proved difficult to realize [18].

The cooling ring design that is most similar to our proposed cooling lattices is the RFOFO cooling ring [19]. It consists of solenoids tightly interleaved with (overlapping, in fact) RF cavities. Injection into that lattice was studied by removing RF cavities from the injection region. The result was a significant loss of performance, and an extremely powerful kicker was required.

Clearly the biggest challenges in these cooling rings have been injection and extraction. Attempts to add injection to a design, which has little space in its basic lattice cell have negatively impacted performance. We propose a design, which has a long straight section in its cell structure. While some of that straight section will be used for RF, the remainder can be left open for injection/extraction kickers. We also suggest that in place of a septum, a superconducting flux pipe [20] be used to bring the injected beam close to the circulating beam and thus reduce the strength required for the kicker.

We examine here the possibility of utilizing a lattice based on dipoles to provide dispersion and solenoids to provide focusing but with the additional attribute that the bending arcs be achromatic. This allows one to provide longer straight sections between the bending arcs and also to easily exercise the option to reverse the bending directions of subsequent arcs. Thus, additional flexibility to the layout of the system is provided allowing the use of completely open structures in which injection into and ejection out of a ring are not required. We describe the lattice and the beam dynamics of this dipole-solenoid system. We also show the results of 6D cooling simulations with liquid hydrogen absorbers installed.

2. The achromatic solenoid-dipole ring cooler

The basic cell structure we propose consists of an arc and a straight section. The arc is achromatic at a particular reference energy, which allows the cell to be used in a closed ring or in an open single-pass configuration, and even to switch between the two. Transverse focusing is primarily provided by solenoids, and

bending is provided by the dipoles in the arcs. Wedge-shaped absorbers are placed in the arcs where there is dispersion, while RF cavities are in the straight sections. We envision a series of rings for cooling from large to small emittances, with an open version of the lattice matching (and probably cooling) the beam between stages. We show a schematic of the ring cooler in Fig. 2 with an injection system that uses a superconducting flux pipe.

The lattice design has evolved from the original concept shown in Fig. 2 to a lattice design that is much more effective for cooling. Our first design of an achromatic cooling lattice, which had a two-sided "racetrack" shape, had rather poor cooling performance. We identified two causes for this: a very low dynamic aperture, and a small momentum passband. Particles that were lost showed significant signs of coupling between the transverse and longitudinal planes. Furthermore, since the minimum of the time-of-flight as a function of momentum was at a relatively low momentum, we were forced to operate at a low momentum (145 MeV/c) to stay on one side of the minimum so as to have synchrotron oscillations. These observations, plus experience from the RFOFO cooling ring [19] that dynamic aperture was reduced when there was more bending, led us to reduce the dispersion in the ring using a four-sided shape, but otherwise the same structure. This would allow us to operate at a higher momentum, improving the sum of the damping partition numbers [4]. We also designed the lattice so that the tune was 1.75 (instead of the original 1.68), so as to center the design momentum in the passband. The dynamic aperture did not improve when we did this, indicating that the dynamic aperture was dominated by the solenoid part of the lattice, and that the symmetry breaking from the bending was a minor contribution.

We then made a modified lattice where each superperiod was close to having an internal eight-fold symmetry (see Figs. 3 and 4). The original lattice lacked this symmetry since it was desirable to have a long distance between solenoids in the straight sections to allow space for injection and extraction hardware, while it was desirable to have low beta functions at the absorbers in the arcs. The resulting lattice had a significantly improved dynamic aperture, and a significantly improved momentum passband arising from the reduced chromaticity of the lattice. In addition, we used a four-sided lattice to improve the sum of the damping partition numbers as described above. The resulting cooling performance was a significant improvement over that of the original lattice.

In Fig. 5, we show the ring quadrant for the four-sided solenoid-dipole ring cooler. This four-sided ring has four 90° arcs with 8 dipoles separated by solenoids in each arc. The arcs are achromatic both horizontally and vertically. The result is that the dispersion is zero in the straight sections between the arcs. To generate dispersion primarily in one of the two transverse phase space planes, thereby simplifying the task of making the arc achromatic, we alternate the field directions of successive solenoids. In Table 1, we
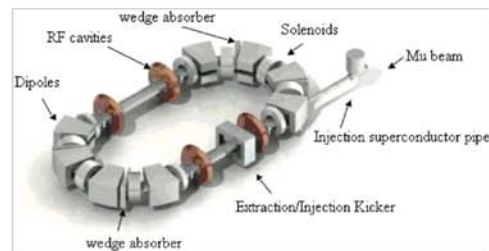

Fig. 2. Schematic drawing of an achromatic 6D ring cooler with superconducting flux pipe injection system.

provide the lattice parameters for this design. In Fig. 6, we show the dynamic aperture at a working momentum of 220 MeV/c. The normalized action in the plot is defined as follows: if M is the 4×4 linear map for the transverse variables about the energy-dependent cl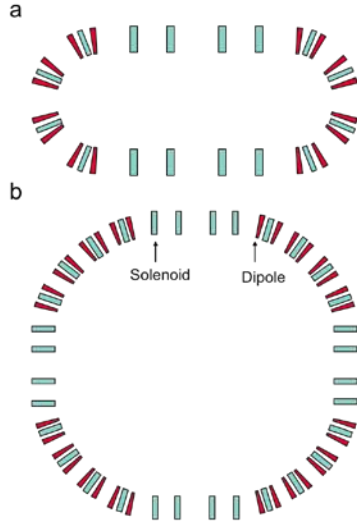osed orbit, define A to be a symplectic matrix that block-diagonalizes M, with the blocks being 2×2 rotation matrices ($A^{-1}MA = R$, where R is the block-diagonal matrix). The phase space variables for M should be coordinates and momenta divided by mc, where m is the particle mass and c is the speed of light. If a particle has a phase space vector z, and $u = A^{-1}z$, then the normalized actions are $(u_1^2 + u_2^2)/2$ and $(u_3^2 + u_4^2)/2$. If the beam were matched to the lattice, the average of the normalized actions would be the transverse normalized emittances.

3. Beam dynamics in the 6D cooling ring

After linear lattice solutions of the four-sided ring cooler are obtained using the code SYNCH [21], we perform tracking simulations using ICOOL [22]. Our working momentum of the muons is chosen to be 220 MeV/c. In order to cool the beam, liquid hydrogen (LH$_2$) wedge absorbers are inserted into a region with low β and high dispersion. In the arcs, the absorbers occupy

Fig. 3. Schematic drawing of the modified racetrack achromatic ring (top) and four-sided ring (bottom) utilizing dipoles and solenoids.
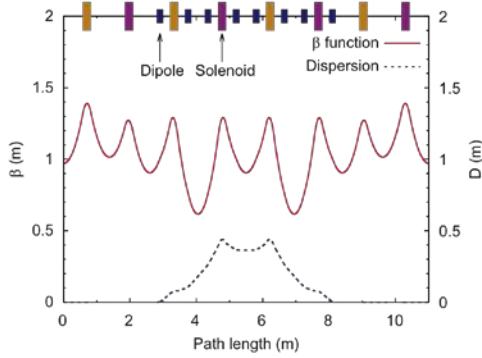
Fig. 4. Beta function and dispersion of the four-sided ring.

Table 1
Parameters of the four-sided and achromatic ring cooler.

Momentum (MeV/c)	220
Superperiods	4
Number of dipoles	32
Number of straight solenoids	16
Number of arc solenoids	16
Arc length (m)	6
Straight section length (m)	5
Dipole length and field	0.2 m, 0.72,045 T
Dipole bend and edge angles (deg.)	11.25, 2.8,125
Arc solenoid length and field	0.25 m, 3.38,290 T
Straight section solenoid length and field	0.25 m, 2.91,555 T
Superperiod length and xytunes	11 m, 1.75
Circumference (m)	44
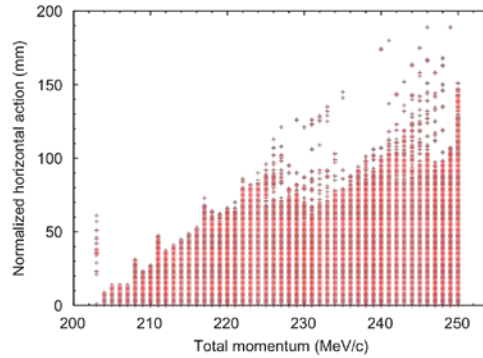
Fig. 6. Dynamic aperture for the four-sided ring cooler at working momentum of 220 MeV/c. There is no dynamic aperture below 201 MeV/c or above 250 MeV/c due to integer and half-integer stopbands, respectively, arising from the dependence of the tune on momentum.
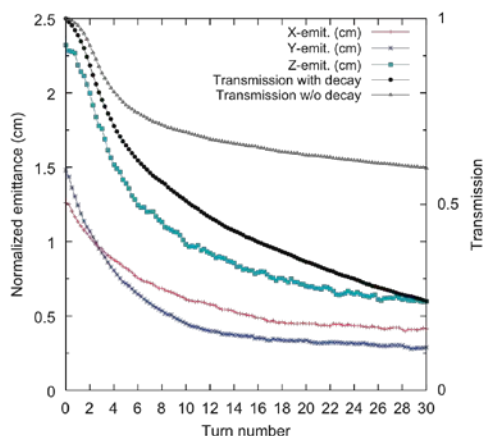

Fig. 5. Schematic drawing of the ring quadrant in the four-sided and achromatic ring cooler.

Fig. 7. Beam emittance and transmission as a function of full ring turns.
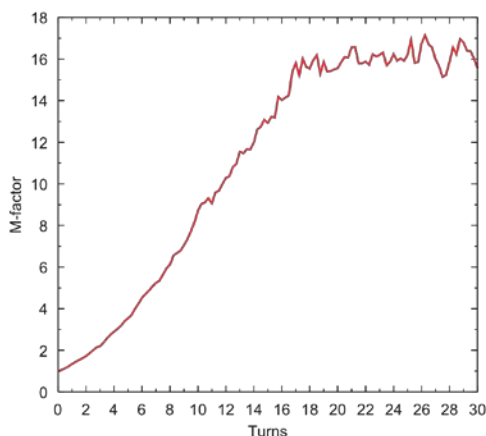

Fig. 8. Merit factor [19] (see text above) with muon decay considered.

Table 2
Beam parameters vs. number of turns.

Number of turns	0	15
Normalized horizontal emittance (cm)	1.26	0.51
Normalized vertical emittance (cm)	1.48	0.36
Normalized longitudinal emittance (cm)	2.32	0.81
Transmission (%) without decay	100	65.9
Transmission (%) with decay	100	41.3

the straight sections between the second and third dipole and between the sixth and seventh dipole. Each LH_2 wedge absorber has a length of 19.5 cm along the closed orbit of the working momentum. The energy loss rate at the absorber is 0.303 MeV/cm and the total angle of each wedge is 23°. Four 201.25 MHz accelerating cavities (RF) are placed in the superperiod. Each cavity has a maximal axial accelerating gradient of 15 MV/m and the RF phase is set at 30°. The RF cavities will restore the energy of the muon beam as it is lost in the LH_2 absorbers. The four-sided ring has positive dispersion, and the absorber wedges are oriented such that higher-energy particles traverse more absorber material and thus they lose more energy per turn than the lower energy particles do. Consequently, cooling takes place in the longitudinal as well as the transverse dimensions.

Evolution of the beam parameters in the cooling process during 30 turns of the four-sided ring cooler is presented in Fig. 7. The initial input beam is selected by first generating a beam with large spreads in all 6 dimensions and following the passage of each particle through 15 full-turns of the ring with stochastic processes (multiple Coulomb scattering and energy straggling) turned off. We then identify the beam particles which successfully traverse the complete 15 turns of the ring and recover their initial starting values. We then re-launch these recovered particles with the stochastic processes turned on. The initial and final beam parameters for the 6D cooling are given in Table 2. Note that the emittance reduction is confined mainly to the first 15 full-turns of the ring at which point the emittances are approaching an equilibrium value for each of the three dimensions. The cooling rate in the vertical plane is higher than that in the horizontal plane, and the equilibrium emittance in the vertical plane is lower than that in the horizontal plane. This is because

the dispersion and wedges primarily couple the horizontal and longitudinal planes together, and thus the longitudinal plane achieves its cooling primarily at the expense of the cooling in the horizontal plane. One could potentially create a more equal performance in the two transverse planes by generating dispersion in both transverse eigenplanes, which will be a subject for future studies.

We also compute the merit factor as defined in [19]. This factor is the ratio of the initial product of the horizontal, vertical, and longitudinal emittances to the final value of that product, multiplied by the fraction of the muons that survive. This merit factor vs. the number of turns is shown in Fig. 8. While this merit factor appears to compare poorly to those of other lattices [10,15,17,19], the performances become more comparable once those other lattices make provisions for injection [11,19] (our lattice already has space set aside for that). Furthermore, we have not yet completed a full optimization of parameters for this lattice, and we expect to achieve improved performance by doing so.

4. Conclusions

We have described an achromatic ring cooler using solenoids and dipoles as lattice elements. Beam dynamics simulations show that the four-sided ring has a substantial dynamic aperture. In addition, the insertion of LH_2 wedge absorbers into the arcs of this ring results in the 6D cooling of the phase space of the circulating muon beam.

Acknowledgments

References

[1] Proceedings from the First Workshop on Muon Colliders Napa, California, 1992, Nucl. Instr. and Meth. A350 (1994) 24; P. Chen, K. MacDonald, Summary of the physics opportunities working group, in: J. Wurtele (Ed.),

19

Proceedings of the 1992 Advanced Accelerator Concepts Workshop, Port Jefferson, NY. AIP Conf. Proc. 279 (1993); Physics potential and development of $\mu^+\mu^-$ colliders, in: D. Cline (Ed.), Proceedings of the 2nd Workshop, Sausalito, CA, AIP Conf. Proc. 352 (1995); Beam dynamics and technology issues for $\mu^+\mu^-$ colliders, in: J. Gallardo (Ed.), Proceedings of the 9th Advanced ICFA Beam Dynamics Workshop, AIP Conf. Proc. 372 (1996); Physics Potential and Development of $\mu^+\mu^-$ Colliders, San Francisco, CA, December 1997, D. Cline (Ed.), AIP Conf. Proc. 441 (1998).

[2] M. Yu, Ado, V.I. Balbekov, Sov. At. Energy 31 (1971) 731.
[3] A.N. Skrinsky, V.V. Parkhomchuk, Sov. J. Part Nucl. 12 (1981) 223.
[4] D. Neuffer, Part. Accel. 14 (1983) 75.
[5] D.V. Neuffer, R.B. Palmer, A high-energy high-luminosity muon collider, in: Proceedings of the 1994 European Particle Accelerator Conference, London, UK, 1994.
[6] S. Geer, Phys. Rev. D57 (1998) 6989.
[7] M. Alsharo'a, et al., Phys. Rev. Spec. Top. Accel. Beams 6 (2003) 081001.
[8] V.I. Balbekov, A. Van Ginneken, Ring cooler for muon collider, in: David B. Cline (Ed.), Physics Potential and Development of $\mu^+\mu^-$ Colliders: Fourth International Conference, AIP Conference Proceedings 441, American Institute of Physics, 1998, pp. 310–313.
[9] V.I. Balbekov, Possibility of using a ring accelerator for ionization cooling of muons, in: A. Luccio, W. MacKay (Eds.), Proceedings of the 1999 Particle Accelerator Conference, New York, IEEE, Piscataway, NJ, 1999, pp. 315–317.
[10] V. Balbekov et al., Muon ring cooler for the MUCOOL experiment, in: P. Lucas, S. Webber (Eds.), Proceedings of the 2001 Particle Accelerator Conference, Chicago, IEEE, Piscataway, NJ, 2001, pp. 3867–3869.
[11] V. Balbekov, Ring Cooler Progress, NFMCC-doc-246, 2002, ⟨http://nfmcc-docdb.fnal.gov/cgi-bin/DocumentDatabase/⟩.
[12] Steve Kahn, Hard Edge Simulation of TETRA Ring in GEANT (again), Presentation at the Theory and Simulation Meeting, LBNL, October 21, 2002, ⟨http://www.cap.bnl.gov/mumu/conf/thsim-021021/⟩.
[13] Zafar Usubov, GEANT-3.21 Simulation of the Balbekov Square Cooling Ring, Presentation at the Ring Coolers/Emittance Exchange Group Meeting, April 1, 2003, ⟨http://www.fnal.gov/projects/muon_collider/eexchange/Meetings/Meeting36/agenda.htm⟩.
[14] Harold G. Kirk, et al., Progress towards a muon ring cooler, in: Norman Graf (Ed.), Proceedings of Snowmass 2001, 2002, M101, ⟨http://www.slac.stanford.edu/econf/C010630/⟩.
[15] Harold Kirk et al., Muon storage rings for 6D phase-space cooling, in: Joe Chew, Peter Lucas, Sara Webber (Eds.), Proceedings of the 2003 Particle Accelerator Conference, IEEE, Piscataway, NJ, 2003, pp. 2008–2010.
[16] D.J. Summers, et al., Int. J. Mod. Phys. A 20 (2005) 3851.
[17] H.G. Kirk et al., A Compact 6D Muon Cooling Ring, in: C. Horak (Eds.), Proceedings of 2005 Particle Accelerator Conference, Knoxville, Tennessee, IEEE, Piscataway, NJ, 2005, pp. 3025–3027.
[18] S.A. Kahn et al., Design of a magnet system for a muon cooling ring, in: C. Horak (Eds.), Proceedings of 2005 Particle Accelerator Conference, Knoxville, Tennessee, IEEE, Piscataway, NJ, 2005, pp. 3366–3368.
[19] R. Palmer, et al., Phys. Rev. Spec. Top. Accel. Beams 8 (2005) 061003.
[20] F. Martin, S.J. St. Lorant, W.T. Toner, Nucl. Instr. and Meth. 103 (1972) 5033 103 (1972) 503.
[21] A.A. Garren, A.S. Kenney, E.D. Courant, A.D. Russell, M.J. Syphers, SYNCH, A program for Design and Analysis of the Synchrotrons and Beamlines, LBL-34668, BNL-49925, FNAL-PUB-94/013, 1993.
[22] R.C. Ferrow, ICOOL: a simulation code for ionization cooling of muon beams, in: C.A. Luccio, W. Mackay (Eds.), Proceedings of the 1999 Particle Accelerator Conference, New York, 1999, p. 3020.

20

Optimization of a mercury jet target for a neutrino factory or a muon collider

X. Ding,[1,*] J. S. Berg,[2] D. Cline,[1] and H. G. Kirk[2]

[1]University of California at Los Angeles, Los Angeles, California 90095, USA
[2]Brookhaven National Laboratory, Upton, New York 11973, USA

A study of target parameters for a mercury jet target for a neutrino factory or muon collider is presented. We simulate particle production initiated by incoming protons with kinetic energies between 2 and 100 GeV. For each proton beam kinetic energy, we maximize production by varying the geometric parameters of the target: the mercury jet radius, the incoming proton beam angle, and the crossing angle between the mercury jet and the proton beam. With an 8-GeV proton beam, we study the variation of meson production with the entry direction of the proton beam relative to the jet. We also examine the influence on the meson production by the focusing of the proton beam. The number of muons surviving through the neutrino factory front end channel is determined as a function of the proton beam kinetic energy.

DOI:

PACS numbers: 29.20.db, 29.27.Eg, 29.25.Pj, 13.20.Cz

I. INTRODUCTION

Future facilities based on intense beams of muons—the muon collider and the neutrino factory—offer the promise of extraordinary physics capabilities [1,2]. The muon collider (MC) provides a possible approach to a multi-TeV lepton collider, and hence a way to explore new physics beyond the reach of present colliders. In addition, a neutrino factory (NF) gives the opportunity to perform extremely sensitive neutrino oscillation experiments while also opening expanded avenues for the study of new physics in the neutrino sector.

MC and NF accelerator complexes are shown schematically in Fig. 1 [1,3,4]. Both the MC and NF require a target solution that can convert a multi-MW proton beam into an intense muon source. The requirements for a muon collider and a neutrino factory capable of delivering a large number of muons in order to achieve acceptable performances pose significant challenges to a target. For instance, the target must be a high-Z material in order to produce pions copiously, yet not be so large as to result in a significant rate of absorption of secondary pions within the target material. Second, the target system must survive in the extreme conditions of a powerful MW-class proton beam, where the target will have to dissipate large amounts of energy, survive the strong pressure waves induced by the short beam pulses, and also survive long-term effects of radiation damage. A concept of utilizing a free-flowing mercury

jet target has been proposed to accomplish the task [5]. The MERIT collaboration [6] built such a target and tested it with an intense proton beam. The experiment validated the concept of a free mercury jet inside a high-field solenoid magnet as a target for a pulsed proton beam of 4-MW power. Figure 2 shows a schematic of the target concept. The target is inside solenoids that generate a 20-T magnetic field that tapers to lower values of 1.5 T for $z > 15$ m [5]. Pions are produced when a proton beam is delivered onto the mercury jet target. The pions are captured in the high-field solenoids and then transported into a decay channel in which the pions decay to produce both positive and negative muons.

The production of pions at the target depends on the size of the target, the orientation of the proton beam relative to the magnetic field, and the angle of the beam and jet relative to each other. In the present paper, we will report our efforts on the meson production simulations for this mercury jet target to provide an optimized solution for the conversion of a powerful MW-class proton beam into an intense muon beam. The meson production is defined to be the collection of charged muons and charged pions at the end of a 50 m decay channel. In this paper, Sec. II describes an optimization study of these geometric target parameters for the liquid mercury jet target system and the meson production efficiencies as a function of the primary proton kinetic energy. In Sec. III, we examine the correlation between meson production and multiple beam entry points for the proton beam onto the jet. In Sec. IV, we present the relation between the β^* of the focused proton beam and the resulting meson production. In Sec. V, we determine the number of muons surviving through the NF front end channel as a function of the proton beam energy and, finally, we conclude with a summary in Sec. VI.

---

*Corresponding author.
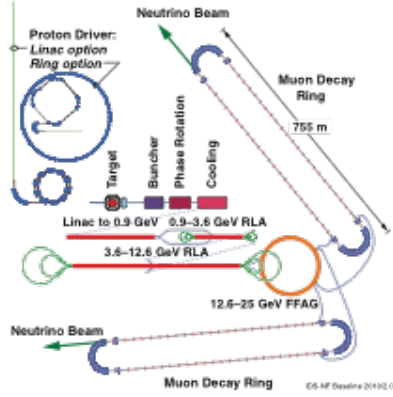xding@bnl.gov.

© 2011 American Physical Society

21

FIG. 1. Schematic of a 25-GeV NF (top); schematic of a 1.5-TeV MC (bottom).

II. OPTIMIZATION OF GEOMETRIC TARGET PARAMETERS AND MESON PRODUCTION EFFICIENCY AS A FUNCTION OF PROTON BEAM KINETIC ENERGY

The mercury jet target geometry is shown in Fig. 3. For this series of simulations the proton beam is launched under the mercury jet at $z = -75$ cm. The proton beam and mercury jet will intercept at (0 cm, 0 cm, -37.5 cm). We run MARS15 [7], a Monte Carlo code capable of simulating particle interactions and transport, and count all the mesons that cross a transverse plane 50 meters downstream from the beam/jet interaction. We then select the muons whose kinetic energies are in the range of 40 to 180 MeV. This is done because we find that the number of mesons in
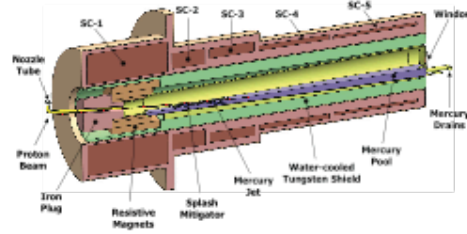
FIG. 2. Concept of a 4-MW target station with a continuous mercury jet target for an intense proton beam. The mercury jet is tilted by 100 mrad with respect to a 20-T solenoid magnet that captures and conducts low-momentum pions into a decay channel. The mercury is collected in a pool that also serves as the proton beam dump.

this kinetic energy band is proportional to the number of mesons which eventually survive the subsequent downstream phase rotation and transverse cooling sections, independent of other parameters such as the proton beam kinetic energy and target geometry [8].

To find the optimal values for the geometric parameters, we first make several simulations with different values for a single parameter. We then fit a curve (using least-squares fitting with a third order polynomial) through the data for meson production (with uncertainties, which can be computed from the MARS15 results since each incoming beam proton is independent) as a function of the parameter in question. We take the parameter value at the maximum in the fitted curve to be the current optimal value for that parameter. We repeat this process for each parameter, and then cycle through the parameters again until the parameter values have converged. As a result of the least-squares fitting process, we are able to obtain uncertainties in the optimal parameter values and the production values.

The parameters we vary are shown in Fig. 4. They are the jet radius, the angle between the proton beam and the magnetic field at $z = -75$ cm, and the angle between the jet and the proton beam at their intersection point, $z = -37.5$ cm. The proton beam is Gaussian, with an rms radius set to 0.3 times the target radius. When the proton beam angle relative to the magnetic field is adjusted, care is
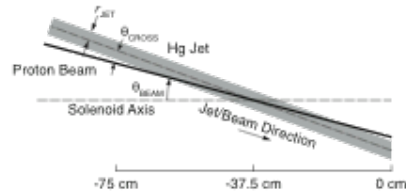

FIG. 3. The mercury jet target geometry. The proton beam and mercury jet cross at $z = -37.5$ cm.

taken to ensure that the launch positions and directions at $z = -75$ cm are properly set so that the beam/jet intercept is always at $x = y = 0$ cm. For each energy, we start with the proton beam at an angle of 67 mrad with respect to the magnetic field, a crossing angle of 33 mrad between the jet and the proton beam, and a target radius of 5 mm [5,9].

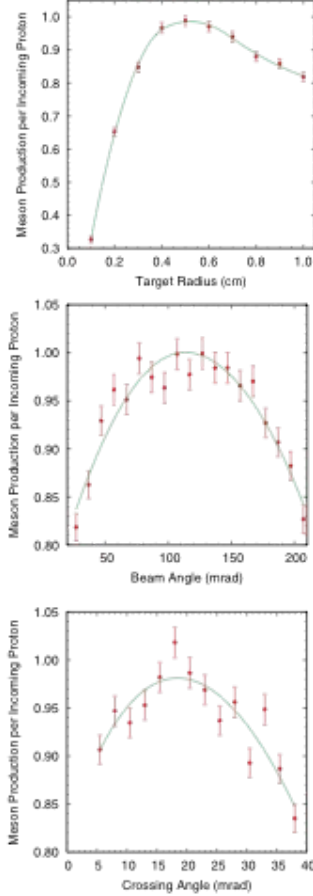Using the described optimization method (an example shown in Fig. 5), we get the optimal values and the uncertainties for target radius, beam angle at $z = -75$ cm,

FIG. 5. The optimized proton beam angle in each cycle (top) and meson production as a function of the iteration number during the optimization procedure (bottom). The meson production corresponding to the optimized proton beam angle in each cycle is run at No. 2, No. 5, No. 8, No. 11, and No. 14. Data points are generated from 2×10^5 incoming 8-GeV protons.

and crossing angle at the beam/jet intercept point of $z = -37.5$ cm for proton kinetic energies between 2 and 100 GeV. These results are shown in Fig. 6. Figure 7 shows meson production before and after optimization for proton energies between 2 and 100 GeV. Each curve has been normalized to the beam power. We see that the meson production is most efficient near proton beam kinetic energies of 8 GeV.

III. MULTIPLE PROTON BEAM ENTRY DIRECTIONS

In the previous section, the proton beam is launched beneath the mercury jet as shown in Fig. 3. Alternative proton beam entry points are also possible. We consider now the case of an 8 GeV proton beam and compare meson production rates for each entry point. Based on the results depicted in Fig. 6, we fix the mercury jet radius to be 0.4 cm and the beam/jet crossing angle at $z = -37.5$ cm to be 27 mrad. The mercury jet angle to solenoid axis is 96.7 mrad. In addition, we define a roll angle to describe on
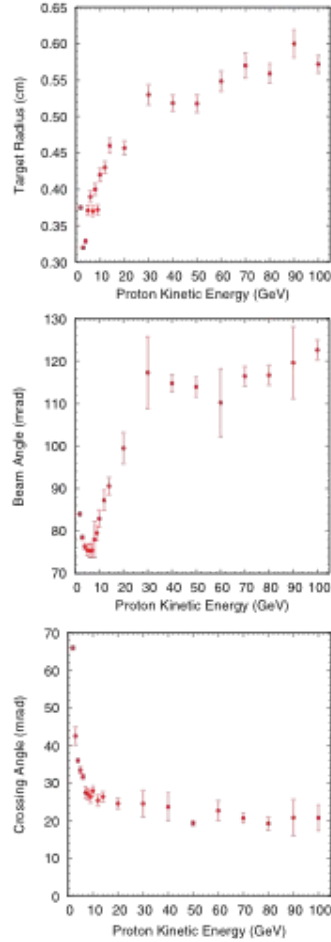

FIG. 4. Meson production as a function of target radius (top), proton beam angle (middle), and beam-target crossing angle (bottom). Data points represent meson production generated from 10^5 incoming 50-GeV protons. Curves are least-squares fits to this data.
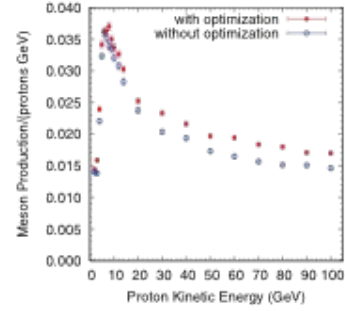
FIG. 7.   Production with original geometry and with optimized geometry.

27 mrad at $z = -37.5$ cm. The proton beams are not all the same distance from the jet at $z = -75$ cm since the proton beam is bent by the magnetic field. For example, at $z = -75$ cm, the (x, y) coordinates of the mercury jet, p0 and p7 are (0, 3.64), (-0.56, 4.62), and (-0.103, 2.638), respectively, in units of cm. All entry directions of the proton beam and mercury jet at $z = -75$ cm are inclined relative to the solenoid axis. The incident beam orientation used in the previous optimization study for the 8 GeV case (grey spot in Fig. 8) is very close to the p6 case. Figure 9 shows the trajectory of the beam relative to the mercury jet in the x-y plane as it moves in z, for various initial beam positions at $z = -75$ cm. Figure 10 shows the clearance and the meson production for various roll angles. We see a

FIG. 6.   Optimized target parameters of target radius (top), beam angle at $z = -75$ cm (middle), and beam/jet crossing angle at $z = -37.5$ cm (bottom) as a function of proton kinetic energy.

which side of the jet the proton beam approaches. The roll angle is defined to be 0 if the proton beam enters the target from above.

We define the clearance to be the distance between the proton beam center and the surface of mercury jet target divided by the rms radius of proton beam. Figure 8 depicts the calculated proton beam positions at $z = -75$ cm for 15 cases each of which keep the same crossing angle of

FIG. 8.   The layout of multiple proton beam entry directions relative to the mercury jet at $z = -75$ cm.
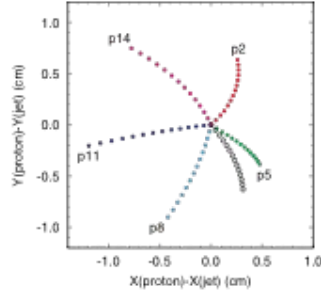
FIG. 9. The trajectory of the 8 GeV proton beam relative to the mercury jet in the x-y plane as the proton moves in z. Points on the outside start at $z = -75$ cm at the labeled positions around the beam (see Fig. 8), and head toward a crossing with the beam at $z = -37.5$ cm (convergence of points in the diagram). Open circles are for the direction for which optimization studies were performed.
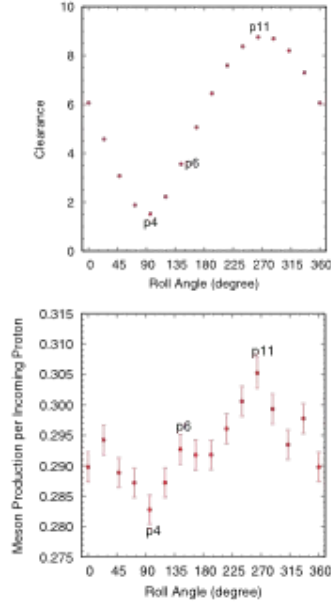

FIG. 10. The clearances (top) and meson production (bottom) for multiple proton beam entry directions relative to the mercury jet at $z = -75$ cm. Data points for meson production are generated from 4×10^5 incoming 8-GeV protons.

correlation between the clearance and the meson production. The peak meson production is 8% higher than for the lowest case and about 4% higher than for the original case with the proton beam entering from below the jet.

IV. FOCUSED INCIDENT PROTON BEAM

Our simulations are based on a simple Gaussian incident proton beam with an infinitely large Courant-Snyder β parameter. We consider now a focused 8-GeV proton beam and study the correlation between the β function of the proton beam and the generated mesons.

In Fig. 11 we show the transverse dimensions of the incident proton beam with a normalized emittance of 25π mm-mrad at three longitudinal positions for the case of horizontal and vertical β functions of 10 cm at $z = -37.5$ cm. We can clearly see the beam is focused and the beam waist is at $z = -37.5$ cm. Figure 12 shows the meson production as a function of β^* of the proton beam. We see that the meson production loss is negligible (< 1%) for $\beta^* \geq 0.3$ m.
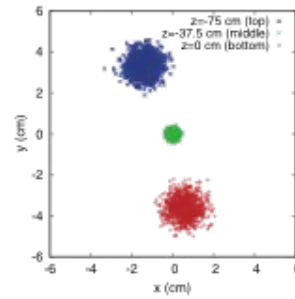

FIG. 11. The x-y plot at three longitudinal positions ($z = -75$ cm, $z = -37.5$ cm, and $z = 0$ cm) with an incident proton beam of normalized emittance 25π mm-mrad and Twiss parameters of $\alpha_x = \alpha_y = 0$, $\beta_x = 10$ cm, and $\beta_y = 10$ cm at $z = -37.5$ cm.
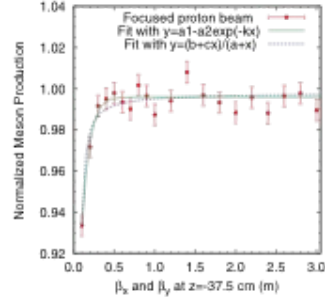

FIG. 12. Meson productions with a Gaussian proton beam, as a function of β_x and β_y at $z = -37.5$ cm. β_x is always set equal to β_y for these simulations.
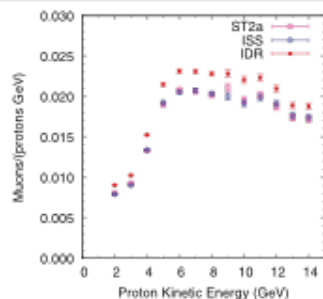
FIG. 13. Muon transmission through the NF front end channel as computed by ICOOL, starting from meson distributions at the downstream end of the target ($Z = 0$ cm).

V. MUON SURVIVAL THROUGH THE NF FRONT END CHANNEL

We compute the number of muons surviving the subsequent phase shaping system for a neutrino factory using version 3.20 of the code ICOOL [10]. We compare the cooling channel performance in the three muon front end lattices (ST2a-BNL for Feasibility Study 2A [11], ST2a-ISS for the International Scoping Study [12], and IDR for the International Design Report of the International Design Study) [13]. The number of muons surviving as a function of the proton beam energy is shown in Fig. 13. We see that the IDR front end lattice has an improved transmission over the ST2a-BNL lattice and the ST2a-ISS lattice. In addition, for constant beam power, the yield is maximum for a beam energy around 7 GeV, but it is within 10% of this maximum for $5 < \text{KE} < 12$ GeV. This result is consistent with the analysis of a tantalum target by Strait *et al.* [14] in which the cross-section data from the HARP experiment [15] was considered.

VI. CONCLUSIONS

We optimize the mercury jet target parameters: the mercury jet radius, the incoming proton beam angle, and the crossing angle between the mercury jet and the incoming proton beam with varying kinetic energies. The optimized target radius varies from about 0.35 to 0.6 cm as the proton beam energy increases. The optimized beam angle at $z = -75$ cm varies from 75 to 120 mrad. The optimized crossing angle at $z = -37.5$ cm is near 20 mrad for energies above 10 GeV. These values differ from earlier choices of 67 mrad for the beam angle and 33 mrad for the crossing angle. These new choices for the beam parameters increase the meson production by about 20% compared to the earlier parameters. Our study demonstrates that the maximum meson production efficiency per unit proton beam power occurs when the proton kinetic energy is in the range of 5–15 GeV.

An examination of multiple proton beam entry directions relative to the mercury jet for the 8-GeV proton beam case demonstrates that an asymmetric layout is required in order to achieve the same beam/jet crossing angle at the jet axis. The peak meson production is 8% higher than for the lowest case and about 4% higher than for the original case with the proton beam entering from below the jet.

An examination of the influence on the meson production by the focusing of the proton beam shows the meson production loss is negligible ($< 1\%$) for a β^* of 0.3 m or higher for the proton beam.

Finally, a simulation of muon transmission through the neutrino factory phase rotation and ionization cooling channel shows that the highest meson production efficiency occurs for proton kinetic energies between 5 and 12 GeV.

ACKNOWLEDGMENTS

[1] Stephen Geer and Michael S. Zisman, Report No. FERMILAB-TM-2459-APC, 2010, https://mctf.fnal.gov/mapproposal.pdf/view.

[2] A. Bandyopadhyay *et al.*, Rep. Prog. Phys. **72**, 106201 (2009) [http://www.iop.org/EJ/article/0034-4885/72/10/106201/rpp9_10_106201.pdf].

[3] M. Apollonio *et al.*, JINST **4**, 07001 (2009).

[4] S. Choubey *et al.* (IDS-NF collaboration), Report No. IDS-NF-017, 2010) [https://www.ids-nf.org/].

[5] S. Ozaki, R. B. Palmer, M. S. Zisman, and J. C. Gallardo, Report No. BNL-52623, 2001.

[6] K. T. McDonald *et al.*, in *Proceedings of the 23rd Particle Accelerator Conference, Vancouver, Canada, 2009* (IEEE, Piscataway, NJ, 2009), p. 795.

[7] N. V. Mokhov, Fermilab-FN-628, 1995; N. V. Mokhov and S. I. Striganov, in *Proceedings of the Hadronic Shower Simulation Workshop, Fermilab* (2006) [AIP Conf. Proc. 896, 50 (2007)], http://www-ap.fnal.gov/MARS/.

[8] X. Ding *et al.*, in Proceedings of the 23rd Particle Accelerator Conference, Vancouver, Canada, 2009 (Ref. [6]).

[9] J. S. Berg *et al.*, Phys. Rev. ST Accel. Beams **9**, 011001 (2006).

[10] R. C. Fernow, in *Proceedings of the 18th Particle Accelerator Conference, New York, 1999*, edited by C. A. Luccio and W. MacKay (IEEE, Piscataway, NJ, 1999), p. 3020.

[11] M. Alsharo'a *et al.*, Phys. Rev. ST Accel. Beams **6**, 081001 (2003).

[12] The International Scoping Study, http://www.hep.ph.ic.ac.uk/iss/.

[13] D. Neuffer *et al.*, in *Proceedings of the 2010 International Particle Accelerator Conference, Kyoto, Japan* (ICR, Kyoto, 2010), p. 3500.

[14] J. Strait *et al.*, Phys. Rev. ST Accel. Beams **13**, 111001 (2010).

[15] M. G. Catanesi *et al.*, Phys. Rev. C **77**, 055207 (2008).

BNL-94919-2011-CP

Muon Collider Final Cooling in 30-50 T Solenoids

Robert B. Palmer, Richard Fernow and Jon Lederman

Physics Department

Brookhaven National Laboratory

U.S. Department of Energy
DOE Office of Science
Dept of High Energy and Nuclear Physics

MUON COLLIDER FINAL COOLING IN 30-50 T SOLENOIDS*

Robert B. Palmer, Richard C. Fernow, BNL, Upton, New York, USA
Jon Lederman, UCLA, Los Angeles, California, USA

Abstract

Muon ionization cooling to the required normalized rms emittance of 25 microns transverse, and 72 mm longitudinal, can be achieved with liquid hydrogen in high field solenoids, provided that the momenta are low enough. At low momenta, the longitudinal emittance rises from the negative slope of energy loss versus energy. Assuming initial emittances that have been achieved in six dimensional cooling simulations, optimized designs are given using solenoid fields limited to 30, 40, and 50 T. The required final emittances are achieved for the two higher field cases.

INTRODUCTION

A multi-TeV muon collider would be smaller, use less power, and hopefully be cheaper than an $e^+ - e^-$ collider with the same performance, but there are significant challenges. Muons are made by pion decay with large emittances. These emittances must be reduced (cooled) in all 6 dimensions.

Reduction of transverse phase space is achieved by ionization cooling[1]. Reduction of longitudinal phase space is achieved using a combination of more transverse cooling, together with emittance exchange. Several schemes have been studied, and two of them [2, 3] appear capable of reducing the emittances to 400 μm transverse, and 1 mm longitudinal (all emittances quoted are rms & normalized). A 1.5 TeV (c-of-m) collider ring has been designed[4] that achieves a luminosity of $1 \times 10^{34} \, cm^{-2} sec^{-1}$, using transverse emittances of 25 μm. This is much less than what is achieved in these 6D cooling schemes. On the other hand the ring can accept a longitudinal emittance of 72 mm, which is much larger than that from the 6D cooling. This allows a complete scheme [5] with final cooling that acts only in the transverse dimensions, while allowing the longitudinal to grow.

The minimum transverse emittances achievable in hydrogen in a long solenoid field B is given by:

$$\epsilon_{x,y}(\min) \; \propto \; \frac{E}{B \, L_R \, dE/dz}$$

where L_R is the material radiation length, dE/dz is the energy loss per unit length, and E is the muon energy. Values of $\epsilon_{x,y}$ for 3 solenoid fields are plotted against energy in Fig.1a. As the muon energy E falls, aided by the increase in dE/dz, the minimum emittance can reach below 25 μm at low enough energies. At these energies, the energy loss (Fig.1b) has a strong negative slope that increases momentum spread, and thus longitudinal emittance. But providing
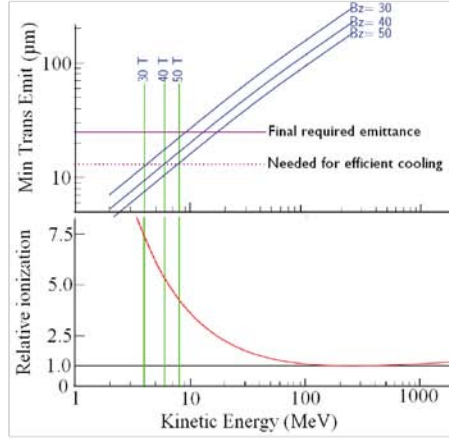
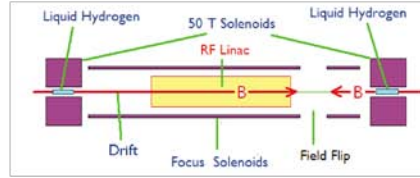Figure 1: a) Minimum transverse emittances vs. muon energy for three magnetic fields; b) energy loss vs. energy.

Figure 2: Schematic of one stage of final cooling.

this slope $-d\epsilon_\parallel/d\epsilon_\perp$ is not too great, the required transverse emittance can be reached with acceptable longitudinal emittance.

FINAL COOLING SEQUENCES

The proposed final cooling system consists of a dozen or so stages. Each stage consists (see Fig. 2) of a high field, small bore solenoid, inside which the muons pass through a liquid hydrogen absorber. Between each solenoid there is rf to re-accelerate and phase-rotate the muons, giving the required energy and energy spread for the following stage. There is also a field reversal to avoid an accumulation of canonical angular momentum. Fig. 3 shows a 40 T example of an ICOOL[6] simulation of the falling energy and transverse emittance, and rising longitudinal emittance.
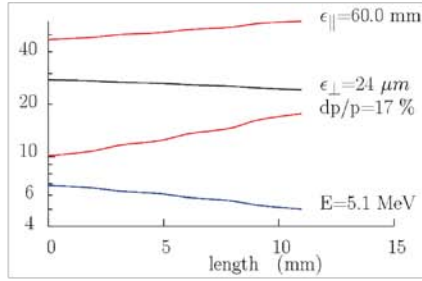
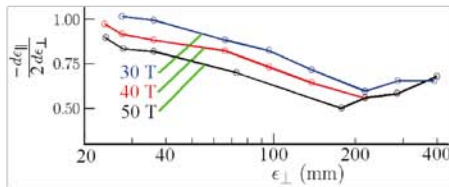Figure 3: Parameters vs. length for ICOOL simulation of cooling in one 40 T solenoid.

Figure 4: One half the ratio of longitudinal to transverse emittance changes vs. representative initial transverse emittances. Values < 1.0 give finite 6D cooling; 1.0 gives constant 6D emittance.

Optimized Stages

For each stage, the initial energy, energy spread, and absorber length, can be adjusted to minimize the ICOOL simulated negative slope $-d\epsilon_{\parallel}/d\epsilon_{\perp}$. Fig. 4 shows negative slopes for manually optimized stages, starting from several representative initial emittances. These were obtained using three different solenoid fields: 30, 40, and 50 T.

Assuming that we can use linear interpolation of the slopes, and other parameters, at intermediate initial emittances, we obtain longitudinal vs. transverse emittances for full sequences using the three fields (see Fig. 5). The sequences start from a transverse emittance of 400 μm, and longitudinal emittance of 1 mm, as achieved at the end of the earlier systems of 6D cooling.

From Fig. 4, we note that, starting from the right ($\epsilon_{\perp}$ = 400 μm), the negative slopes initially fall, i.e. the cooling improves. Here, the bunch length must be kept up to avoid emittance growth from amplitude dependent transit times. With the longitudinal emittance still small, one must use non-optimally small initial momentum spreads dp/p, and low initial energies (67 MeV). As the longitudinal emittance rises, more optimum momentum spreads and initial energies can be used, the cooling becomes more efficient, and the negative slopes fall. In this regime, the advantages of raising the magnetic field are largely cancelled by the worse transit time variations that they produce.
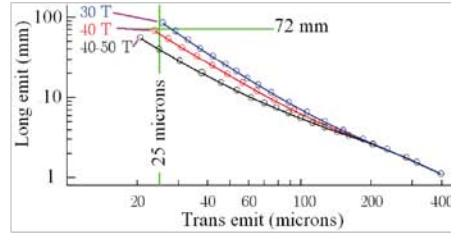

Figure 5: Longitudinal vs. transverse emittances for sequences of stages using three solenoid fields.

Later ($\epsilon_{\perp}$ < 200 μm), when the increased longitudinal emittances allow sufficient bunch length with optimized momentum spreads, getting a low enough equilibrium transverse emittance becomes the dominant problem. For this, the energy must be further lowered, increasing the growth of longitudinal emittance, giving less efficient cooling, and thus rising negative slopes. Now, a higher magnetic field, by reducing the need for lower energies, increases the efficiency, and gives lower negative slopes.

From Fig. 5, we note that the 50 T case more than achieves our requirements, while 40 T just meets them. 30 T just misses the requirement, but could probably be acceptable with some adjustment of parameters.

40 T Example

Fig. 6 shows some parameters vs. stage for the 40 T case. The energy falls in steps from 66 MeV to its final value of 5.1 MeV, while the bunch length rises from 5 to 400 cm. The lengths of hydrogen absorber fall from 77 cm to 1.1 cm, as the energy falls and dE/dz increases. The final beam β is 1.5 cm, giving an rms beam size of 0.6 mm.

Table 1 shows the assumed parameters for the rf. For bunches shorter than 0.75 m, the rf frequencies were chosen to keep $\sigma_{ct} < \lambda/20$. The gradients assumed maximum surface fields $\propto \sqrt{f}$, and, assuming reentrant vacuum cavities with surface to accelerating gradients $\propto f^{0.75}$. For bunches longer than 0.75 m, induction linacs with gradients of 1 MV/m were assumed.

Fig. 7 shows the lengths of the different elements in this example. These are obtained by adding magnet lengths to calculated lengths for phase rotation and re-acceleration. When correctly simulated, the lengths should be shorter because some rotation will occur in the magnet ends, and during acceleration.

The simulated loss, excluding decay, but including 3 sigma cuts, is 17.7 %. The calculated decay loss is 19%, giving a total transmission of 67%.

Matching and Re-acceleration

The matching, re-acceleration and field flips have been fully simulated for only one case: that between the last
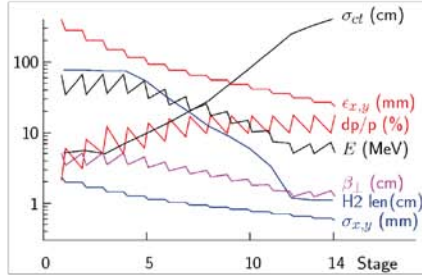
29

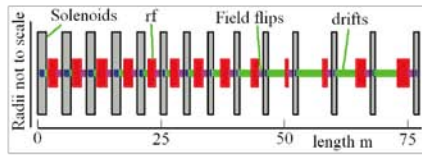Figure 6: Some parameters vs. stage for the 40 T sequence.

Figure 7: Legths of elements in the optimized sequence using 40 T solenoids.
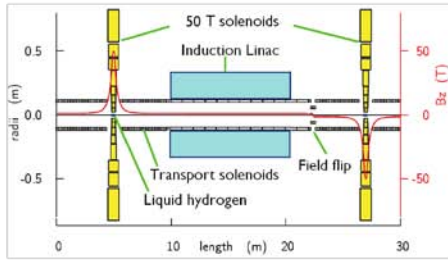

Figure 8: Design of matching and acceleration for the last two stages of the 50 T sequence.
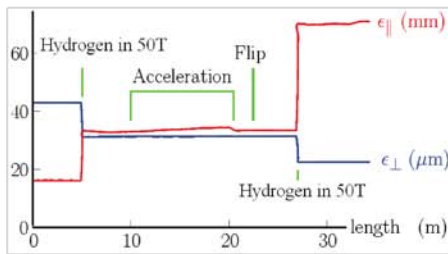

Figure 9: Simulation of matching and acceleration for the last two stages of the 50 T sequence.

Table 1: Rf Parameters of 40 T Example

	E1 MeV	E2 MeV	freq MHz	grad MV/m	acc L m
NCRF	34.6	66.6	201	15.5	2.1
NCRF	34.8	66.9	201	15.5	2.1
NCRF	36.0	67.1	201	15.5	2.0
NCRF	36.0	54.5	153	11.1	1.7
NCRF	30.6	41.3	110	7.4	1.5
NCRF	24.9	32.4	77	4.7	1.6
NCRF	20.7	25.7	53	2.9	1.7
NCRF	17.4	20.0	31	1.5	1.7
Induction	13.6	15.0	18	1.0	1.4
Induction	10.3	10.7	10	1.0	0.4
Induction	7.5	7.2	6	1.0	0.7
Induction	5.1	7.0	5	1.0	1.8
Induction	5.1	7.4	4	1.0	2.3

two stages of the 50 T example. Fig. 8 shows a highly compressed representation of its elements. In this case, the bunch is very long (≈ 3 m), and the rf is an induction linac. Fig. 9 shows the simulated longitudinal and transverse emittances vs. the length. In this example, the simulated emittance dilutions in the acceleration are acceptable: 0.1% transversely and 0.5% longitudinally. The simulated losses are 7.3%, significantly less than the value of 10% estimated from the above assumptions. This is encouraging, but similar simulations of matching and re-acceleration for earlier stages are essential.

CONCLUSION & PROSPECTS

Preliminary simulations of transverse cooling in hydrogen, at low energies, suggests that muon collider emittance requirements can be met using solenoid fields of 40 T or more. It might also be acceptable with 30 T. But these simulations did not include hydrogen windows, matching or re-acceleration, whose performance, with one exception, was based on numerical estimates. Full simulations of more stages are planned. The design and simulation of hydrogen windows must be included, and space charge effects, and absorber heating, calculated.

REFERENCES

[1] G. I. Budker, 1969 Yerevan Conference, AIP Conf. Proc.352 (1996) 4; G. I. Budker, 1970 Kiev Conference, AIP Conf. Proc.352 (1996) 5

[2] R.B. Palmer et al., Phys. Rev. Spec. Top. - Acc. & Beams 8, 061003 (2005).

[3] Y. Derbenev and R. P. Johnson, Phys. Rev. Spec. Top. - Acc. & Beams 8, 041002 (2005).

[4] Y. Alexahin, Proc. 2010 IPAC Conf., p. 1563.

[5] R.B. Palmer et al., A Complete Scheme of Ionization Cooling for a Muon Collider , PAC07 (2007), p. 3193.

[6] R. Fernow, Proc. 2005 Part. Acc. Conf., p. 2651.

MAP Statement of Work
FY12

UCLA

Total: $144K (6 months)

SWF: $134K

Engineers:	0.1 FTE
Technicians:	___ FTE
Scientists:	1.0 FTE
Post Docs:	0.5 FTE
Students:	1

Institution to provide

M&S: $10K

M&S Usage:

(i) MAP-related travel, including MICE operations.
(ii) .

Description of Work:

MAP funds at UCLA are focused on muon collider design studies. Activities include simulations of muon collider cooling channels, including cooling rings and the 40 T final cooling channel. Other work includes optimization studies for high-power MC/NF targets and energy deposition in collider ring magnets.

Milestones* [Description; deliverable; delivery date]:

1. Do production and optimization studies for a gallium target for the MC/NF; report; Q2.
2. Create a systematic algorithm for studying matching between stages of the 40 T final cooling channel; report; Q2.
3. Optimize performance of the dipole-solenoid cooling ring by examining variations in the RF and absorber parameters; report; Q2.

Approvals [Name, Date]:
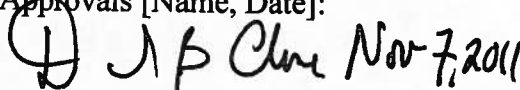
D. Cline Nov 7, 2011

D. Cline
Institutional Representative

S. Geer
MAP Acting Director

---

* Negotiated with L1 managers.